

Article

A Comparative Study on the Effect of Surface and Bulk Sulfates on the High-Temperature Selective Catalytic Reduction of NO with NH₃ over CeO₂

Chong Tan ¹, Zhiwen Gu ¹, Songil Sin ¹, Jiawei Ji ², Yan Wang ¹, Baiyun Zhu ¹, Lijun Cheng ¹, Chunkai Huang ¹, Lulu Li ³, Hongliang Zhang ^{4,*} and Changjin Tang ^{1,5,*}

¹ School of Environment, Nanjing Normal University, Nanjing 210023, China; a1457749802@outlook.com (C.T.); 212502011@njnu.edu.cn (Z.G.); njnu_scr@163.com (S.S.)

² School of Chemistry and Chemical Engineering, Nanjing University, Nanjing 210023, China

³ College of Environmental and Chemical Engineering, Jiangsu University of Science and Technology, Zhenjiang 212000, China

⁴ Analysis and Testing Central Facility, Anhui University of Technology, Ma'anshan 243002, China

⁵ Jiangsu Province Engineering Research Center of Environmental Risk Prevention and Emergency Response Technology, Nanjing 210023, China

* Correspondence: zhanghl@ahut.edu.cn (H.Z.); tangcj@njnu.edu.cn (C.T.); Tel.: +86-25-85891455 (C.T.)

Abstract: Herein, two CeO₂ samples dominantly decorated with surface and bulk sulfates were constructed and their distinct effects on high-temperature NH₃-SCR were investigated by strictly controlling the sulfate content at a comparable level. The obtainment of surface and bulk sulfates was revealed using a designed leaching experiment, and further evidenced by the characterization results from XPS and H₂-TPR. In comparison with CeO₂ modified with bulk sulfates (B-CeS), sufficient acid sites with strong intensity were generated on CeO₂ modified with surface sulfates (S-CeS). In addition, due to electron-withdrawing effect from S=O in sulfate species, NH₃ oxidation over S-CeS was greatly suppressed, providing an additional contribution to enhanced performance in high-temperature NH₃-SCR.

Keywords: CeO₂; high-temperature denitration; surface sulfates; bulk sulfates



Citation: Tan, C.; Gu, Z.; Sin, S.; Ji, J.; Wang, Y.; Zhu, B.; Cheng, L.; Huang, C.; Li, L.; Zhang, H.; et al. A Comparative Study on the Effect of Surface and Bulk Sulfates on the High-Temperature Selective Catalytic Reduction of NO with NH₃ over CeO₂. *Catalysts* **2023**, *13*, 1162. <https://doi.org/10.3390/catal13081162>

Academic Editor: Giuseppe Pantaleo

Received: 6 June 2023

Revised: 20 July 2023

Accepted: 21 July 2023

Published: 28 July 2023



Copyright: © 2023 by the authors. Licensee MDPI, Basel, Switzerland. This article is an open access article distributed under the terms and conditions of the Creative Commons Attribution (CC BY) license (<https://creativecommons.org/licenses/by/4.0/>).

1. Introduction

The large and uncontrolled emission of nitrogen oxides (NO_x, x = 1,2) has caused serious environmental problems, and selective catalytic reduction of NO_x with NH₃ (NH₃-SCR) is testified to be one of the most effective methods for NO_x elimination from stationary sources and diesel vehicles [1]. Among the diverse catalysts developed for NH₃-SCR, the vanadium–titanium system, represented by V₂O₅-WO₃(MoO₃)/TiO₂, has been commercialized for SCR denitration for decades. The operation temperature for V₂O₅-WO₃(MoO₃)/TiO₂ catalysts typically lies in the medium temperature zone (300–400 °C), which is compatible with the flue gas temperature at boiler economizer outlets and thus often used for NO_x removal from coal-fired power plants [2]. However, the installation of this catalyst in high-temperature denitration is largely restrained, mainly due to the aggravated oxidation of ammonia by active V₂O₅ and inferior thermal stability of anatase TiO₂ [3,4]. From the viewpoint of practical application, there is an urgent need for treatment of exhaust gases via high-temperature SCR in some workplaces, such as diesel engines, gas turbines and waste incinerators [5–7].

As early as the 1990s, Topsøe and coworkers pointed out that acid and redox sites are essential for NH₃-SCR catalysts [8,9]. Whether for the Eley–Rideal (E-R) or the Langmuir–Hinshelwood (L-H) reaction pathway, NH₃ adsorption on a catalyst surface constitutes the first step to initiate a reaction. With an increase in reaction temperature, NH₃ adsorption will be disrupted and desorption tends to occur. As such, it is necessary that the catalysts

designed for high-temperature SCR should acquire acid sites with sufficient intensity [10]. On the other hand, their redox properties also need to be carefully regulated, since excessive consumption of NH_3 via heavy oxidation is bound to reduce the available NH_3 for NO reduction. Following these two basic guidelines, a diverse array of catalysts has been explored and such typical combinations like metal ion-exchanged zeolite [11,12] and WO_3/TiO_2 [3,13] are found to exhibit excellent de- NO_x performance even at temperatures higher than 500 °C.

Ceria-based materials, as an important kind of rare-earth oxide, have been extensively studied as efficient V-free NH_3 -SCR catalysts due to their abundant reserve, good redox property and tunable acidity [14,15]. Particularly, by taking advantage of the fascinating characteristics of rich oxygen vacancies and an easy $\text{Ce}^{3+}/\text{Ce}^{4+}$ redox cycle, substantial attention has been paid to CeO_2 for application in low-temperature NH_3 -SCR [16]. Nevertheless, the catalytic behavior at high temperature is less considered. Actually, based on the experimental results of some recent studies, it was shown that by grafting strong acid sites onto the surface of ceria, the NO reduction efficiency at high temperatures (>400 °C) can also be significantly boosted. For example, Yang et al. reported that H_3PO_4 -modified CeO_2 exhibited more than 80% NO conversion in the broad temperature range of 250–550 °C [17]. Our recent study revealed that when applying excessive SO_2 treatment (72 h) over CeO_2 , the obtained catalysts displayed excellent activity at 500 °C with NO conversion exceeding 90% [18].

It is well known that under actual flue gas conditions, SO_2 is widely present. The interaction of SO_2 with CeO_2 will inevitably lead to the generation of sulfate species, and depending on the extent of the interaction, surface sulfates and bulk sulfates are expected to be formed [19,20]. Many previous studies have proved that irrespective of the specific structures or morphologies, sulfate species modification is conducive to enhance the acid strength of CeO_2 and, simultaneously, disrupt the redox properties to a certain extent [21–24]. Obviously, this would endow a positive effect on the performance of high-temperature SCR. However, further details are still lacking. For example, what is the difference between surface sulfate and bulk sulfate species on the catalytic performance of CeO_2 for high-temperature SCR, it is still obscure. Herein, two sulfate species-modified CeO_2 catalysts with comparable sulfur content but distinct existing states were fabricated, and the unique function of surface sulfates and bulk sulfates in high-temperature SCR was explored in detail. Results showed that in comparison with bulk sulfates, surface sulfates played a more significant role in promoting NO conversion at high temperatures, which could be reasonably attributed to the much stronger acid properties and worse redox capacity due to close surface coverage of sulfate species on CeO_2 .

2. Results and Discussion

2.1. Construction of Target Catalysts

The CeO_2 catalysts modified with sulfate species have been widely investigated in NH_3 -SCR, and conventional fabrication is fulfilled according to a bottom-up route, either through vapor sulfation of CeO_2 with $\text{SO}_2 + \text{O}_2$ or via wet impregnation of CeO_2 with $\text{H}_2\text{SO}_4/(\text{NH}_4)_2\text{SO}_4$ [24–26]. Both methods are facile in operation and one can obtain surface or bulk sulfates by tuning the exposure time or modulating the H_2SO_4 concentration. However, it is worth to mention that to explicitly approach the goal of present study, we needed to control the sulfate content at a similar value. This is challenging for the traditional preparation, since bulk sulfates are usually formed at the expense of surface sulfates. In other words, in order to generate bulk sulfates, the introduced sulfur content should be controlled at a very high value. For this reason, an alternative top-down preparation methodology was used to construct the designated catalyst of CeO_2 modified with bulk sulfates.

It is well reported that when CeO_2 is exposed to a feed stream of $\text{SO}_2 + \text{O}_2$ for a short duration, its surface will be covered by an adsorption layer of sulfates [27]. In the present study, this method was utilized to construct the sample of CeO_2 exclusively modified with surface sulfates (S-CeS). However, for the obtainment of CeO_2 modified with bulk sulfates,

the traditional method of treating CeO_2 in a $\text{SO}_2 + \text{O}_2$ stream for a long duration or at a high temperature was not adopted. Alternatively, a novel but facile top-down strategy was performed. That is, directly calcining the sulfated precursor of $\text{Ce}_2(\text{SO}_4)_3 \cdot x\text{H}_2\text{O}$ in air at a high temperature (i.e., 900°C) to convert the majority of metal salts into CeO_2 , and the residual is expected to present mainly as bulk sulfates. Obviously, one notable merit of this method is that it can well resolve the dilemma between low sulfur content and bulk state of sulfates.

To confirm the effectiveness of this method, a TG analysis was first performed. It is clearly visible in Figure 1 that two distinct decomposition processes are displayed. The first step is related to a loss of crystalline water. Compared to desorption of crystalline water, a distinct delay is detected for the thermal decomposition of sulfate species. Evidently, decomposition of sulfate groups cannot be initiated until the temperature reaches 700°C , and a sharp weight loss (29.7%) occurs in the narrow temperature range of $700\text{--}850^\circ\text{C}$. Notably, by inspecting the TG profile at a much higher temperature ($830\text{--}1000^\circ\text{C}$, inset), it is found that the decomposition is still in progress even when the temperature surpasses 900°C . This can satisfactorily explain the existence of minor sulfur in the B-CeS sample after the harsh thermal treatment at 900°C for 1 h.

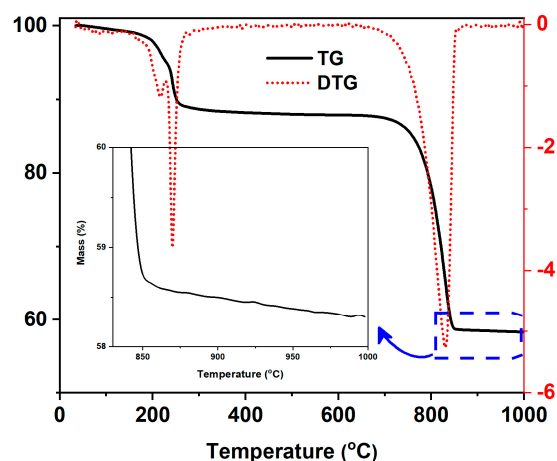


Figure 1. The TG curve of $\text{Ce}_2(\text{SO}_4)_3 \cdot x\text{H}_2\text{O}$ under static air atmosphere. Inset pattern shows the continued process of thermal degradation at $800\text{--}1000^\circ\text{C}$.

EDS analysis (Table 1) was performed to approach the actual sulfur content in B-CeS and S-CeS. It can be seen from SEM images (Figure 2a,b) that due to the employment of different preparation routes, variations in the macroscopic morphology of the two samples are present, and S-CeS exhibits a more porous appearance with fine particles and tight arrangement. From Table 1, a S signal is detected and the measured content displays a low but comparable value (Ce/S ratio: 20.44 vs. 20.78) for B-CeS and S-CeS. Since a variation in the S content is expected to bring great distinction in acid and redox properties [19,27], the construction of sulfate CeO_2 with comparable sulfate loading provides a reliable comparison of the contribution from different sulfate species on the catalytic performance of ceria in high-temperature SCR.

Table 1. Summary of element analysis from EDS and XPS for B-CeS and S-CeS.

Samples	Atomic Concentration (mol.%)				Atomic Ratio (%)		Ce/S *
	Ce	O	S	C	$\text{Ce}^{3+}/(\text{Ce}^{3+} + \text{Ce}^{4+})$	$\text{O}_\beta/(\text{O}_\alpha + \text{O}_\beta)$	
B-CeS	18.42	58.52	2.13	20.93	22.08	33.06	20.44
S-CeS	16.47	54.32	3.6	25.61	40.97	74.07	20.78

* Ce/S ratio determined from EDS analysis.

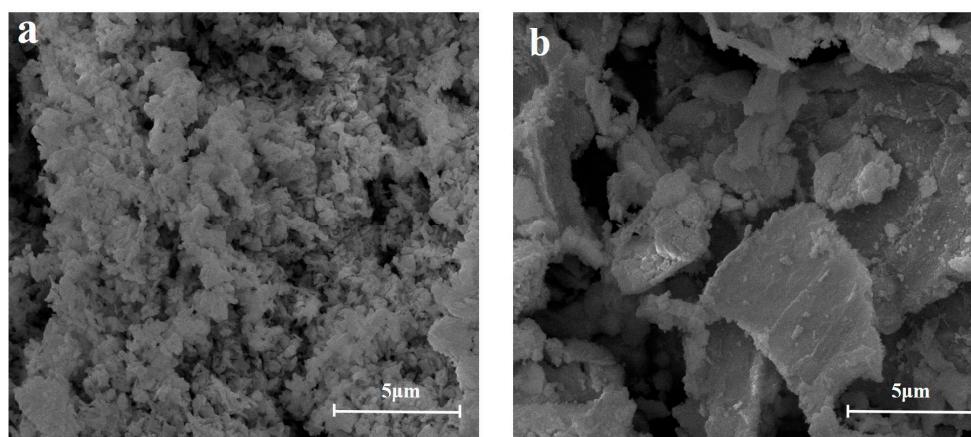


Figure 2. Typical SEM images of (a) B-CeS and (b) S-CeS.

In order to confirm the existence of different sulfate species in B-CeS and S-CeS, a designed water leaching experiment was carried out. According to previous studies, one notable difference between surface and bulk sulfates comes from their solubility in water [19,28]. Commonly, sulfates are tightly bound to a metal oxide surface and cannot be easily leached away by water. Contrarily, analogue to the salt of cerium sulfate, bulk sulfates interact less with the rigid framework of CeO_2 and can thus be easily dissolved in water. Therefore, in the present work, we innovatively utilize this principle to distinguish bulk sulfates and surface sulfates, and with the aid of Raman characterization, the crucial information related to the existing state of sulfates is revealed.

As shown in Figure 3, a sharp band at 463 cm^{-1} , which can be ascribed to the F_{2g} vibrational mode of cubic fluorite CeO_2 , is dominated in the Raman spectra of B-CeS and S-CeS. In addition, no obvious difference in peak intensity is exhibited, suggesting insignificant disturbance on the bulk structure of CeO_2 with sulfate species. By further inspecting the spectra, a weak and broad peak centered around 1170 cm^{-1} is detected and it actually represents the signal from sulfate species [19,29]. Unfortunately, no obvious variation in peak shape or position can be found for B-CeS and S-CeS. Nevertheless, we can still take advantage of the sensitivity of Raman characterization in revealing sulfate signals to approach the crucial information of S content changes. It is observed that the peak intensity of sulfate in B-CeS-W (water leached sample) is significantly lower than that of B-CeS. Interestingly, a negligible change in the peak intensity of the sulfate signal in S-CeS-W is detected as compared to the pristine S-CeS. This sharp difference in the solubility of the sulfate species can be attributed to the different existing states of the sulfate species. That is, bulk sulfates are widely present in B-CeS, while surface sulfates are dominant in S-CeS.

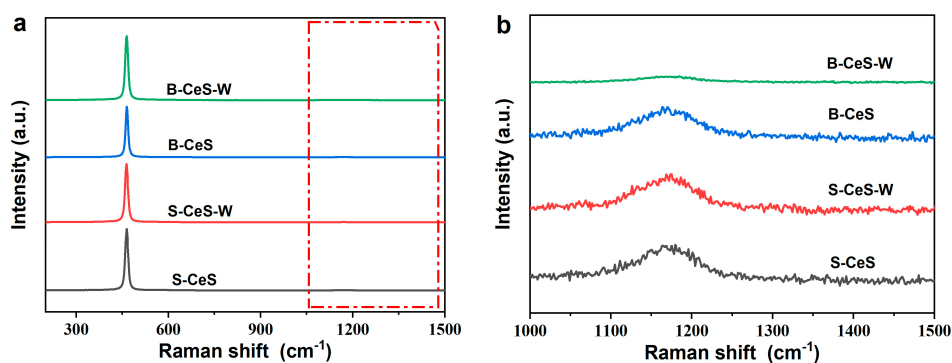


Figure 3. (a) Influence of water leaching treatment on the signal change in Raman spectra for B-CeS and S-CeS. (b) Amplification of Raman signal changes.

2.2. XRD Results

To explore any impact from sulfate introduction on the phase structure of CeO_2 , XRD measurements were performed. It is obvious from Figure 4 that the XRD patterns of B-CeS and S-CeS are represented by the characteristic diffractions from fluorite CeO_2 (JCPDS 43-1002), and no peaks from sulfates are detected. Based on these results, we can conclude that in comparison with Raman, XRD shows less sensitivity in revealing the evolution of sulfate species. For S-CeS, the absence of reflection peaks from cerium sulfate is understandable, since the sulfates are well dispersed on CeO_2 . However, for B-CeS, we suppose the absence of signal from cerium sulfate is mainly due to the low loading or amorphous structure [29].

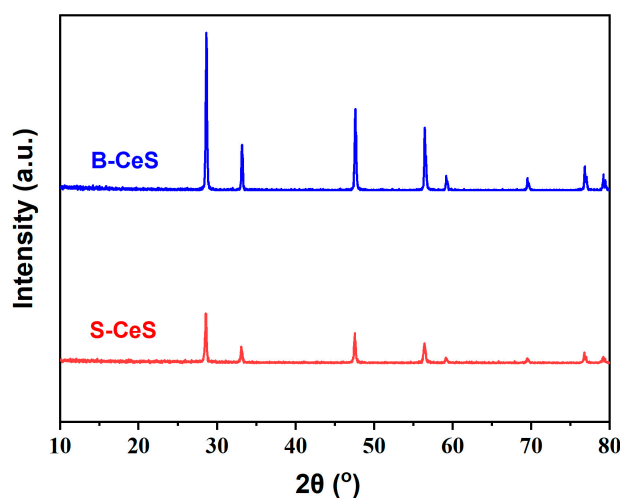


Figure 4. The XRD patterns of S-CeS and B-CeS.

When it comes to the signal related to CeO_2 , a clear difference is exhibited. In general, the appearance of sharp peaks suggests high crystallinity of CeO_2 in both catalysts. This is basically in agreement with the high-temperature treatment and small surface area shown by the two catalysts (B-CeS: $3.6 \text{ m}^2/\text{g}$, S-CeS: $10.8 \text{ m}^2/\text{g}$). Additionally, we can find that although both catalysts are calcined under the same temperature, B-CeS obtains diffraction peaks with a stronger intensity, and the calculated average grain sizes applying the Scherrer equation on the most intense peak at $2\theta = 28.6^\circ$ for B-CeS and S-Ce are 40.2 nm and 31.3 nm, respectively. The results clearly show the sintering behavior of ceria can be influenced by the accompanied anion linked to Ce^{3+} in the precursor.

2.3. XPS Measurement

To obtain a better understanding of the chemical state of elements on the catalyst surface, XPS characterization was performed. Figure 5a presents the S 2p spectra. No obvious difference in the binding energy of S is exhibited, and the appearance of a typical band at 168.7 eV conveys the sulfur element is in the oxidation state of +6, in accordance with the formation of SO_4^{2-} [30]. In addition, a smaller surface atomic concentration of S is observed for B-CeS (2.13%) when compared to S-CeS (3.60%). This can be viewed as convincing evidence for the aggregated feature of sulfate species in B-CeS sample.

The XPS spectra of Ce 3d are shown in Figure 5b. The peaks denoted as u' and v' are related to Ce^{3+} species, and u , u'' , u''' , v , v'' and v''' are attributed to Ce^{4+} species. From Table 1, we can see that the introduction of surface sulfate species induces a significant augmentation of the surface concentration of Ce^{3+} . This is not surprising since Waqif et al. reported that SO_2 can act as a reducing agent and lead to the formation of $\text{Ce}_2(\text{SO}_4)_3$ on a CeO_2 surface [31]. Additionally, the obtainment of a much higher surface Ce^{3+} concentration can be attributed to the fact that most S in S-CeS are concentrated on the surface with CeO_2 , and therefore more surface Ce^{3+} are generated.

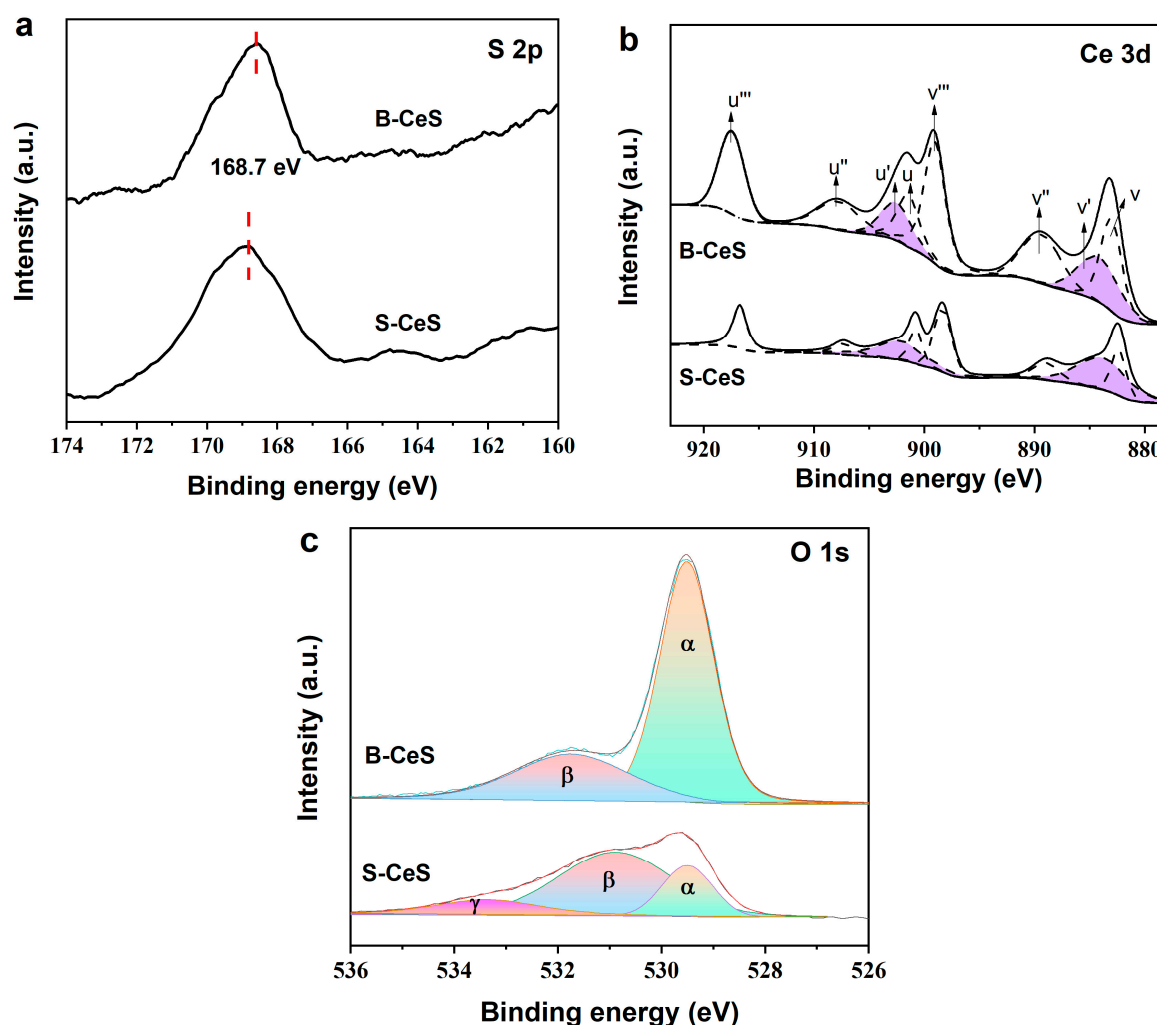


Figure 5. The XPS spectra of (a) S 2p, (b) Ce 3d and (c) O1s for B-CeS and S-CeS.

Regarding the O 1s spectra, a significant difference in the peak shape is displayed. For B-CeS, two well resolved peaks are detected, and they can be reasonably attributed to the signals from lattice oxygen O_{α} (529.0–530.0 eV) and surface oxygen O_{β} (531.3–531.9 eV). Owing to insufficient contact of the CeO_2 surface with bulk sulfates, O_{β} shows a much weaker intensity than O_{α} . However, the case is very different for S-CeS. O_{β} undergoes an obvious enhancement with the surface coverage of sulfates. In addition, a third peak, O_{γ} , located at the binding energy of 532.7–533.5 eV, springs out. According to a previous study, this peak can be related to the signal from surface hydroxyl species [32]. Based on the XPS analysis, we know that the different existing states of sulfate species induce a lot of alteration on the surface features of CeO_2 , and this is particularly true for the S-CeS sample. For B-CeS, lattice oxygen species from ceria are dominant, while the surface oxygen species from sulfate are enriched in S-CeS.

2.4. H_2 -TPR Results

To explore the impact from varied sulfate species on the reduction behavior of CeO_2 , H_2 -TPR was carried out and is shown in Figure 6. According to previous reports, three species have potential for interaction with H_2 over the catalyst of sulfated ceria. They are the surface and bulk oxygen from CeO_2 and the sulfur in sulfates [27,33]. In B-CeS, all of the three reduction peaks are displayed, with corresponding H_2 consumption at low temperatures (peak α , 300–400 °C), medium temperatures (peak β , 450–540 °C) and high temperatures (peak γ , 700–800 °C). For S-CeS, peak γ with a comparable intensity is found.

This is reasonable since this peak is usually attributed to the reduction of bulk oxygen in the deeper interior of CeO_2 . However, for the other two peaks, significant changes are displayed. That is, peak α cannot be observed anymore and peak β shifts to higher temperatures, with its signal strongly intensified.

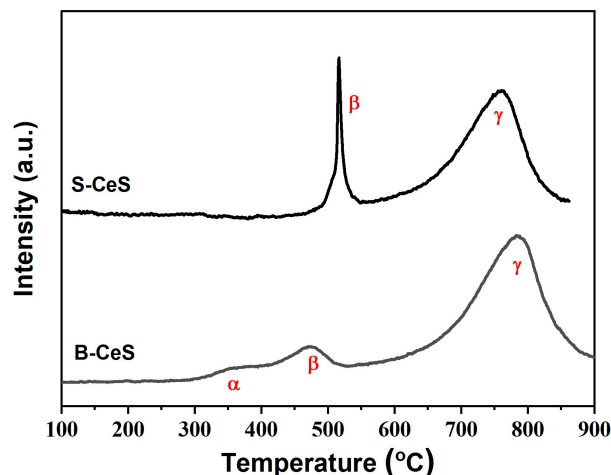


Figure 6. The H_2 -TPR patterns of B-CeS and S-CeS.

It is well known that for pure CeO_2 free from any alien element modification, in addition to the reduction of bulk oxygen, the reduction of surface oxygen at a much lower temperature usually accompanies it [33]. This feature is shown by the appearance of a minor peak centered at 360°C for the B-CeS sample (peak α). However, for S-CeS, the peak α disappears. In view of the fact that surface sulfate species are abundant, we suppose that the disappearance of the reduction peak from oxygen species on the ceria surface actually reflects that most of them reacted with SO_2 in generating surface sulfate species. This can also explain the presence of the large β peak shown for the S-CeS sample.

Based on the comprehensive characterizations using Raman, XPS and H_2 -TPR, it is concluded that two kinds of sulfate species are established for CeO_2 . That is, through $\text{SO}_2 + \text{O}_2$ treatment, the surface of CeO_2 is exclusively covered with a layer of sulfate. As a sharp contrast, the sulfate species are present mainly as bulk sulfates through directly calcining $\text{Ce}_2(\text{SO}_4)_3$ at an elevated temperature.

2.5. NH_3 -SCR Performance

The NO conversion and N_2 selectivity as a function of the reaction temperature for pure CeO_2 and sulfated CeO_2 at $200\text{--}500^\circ\text{C}$ is shown in Figure 7a,b. As expected, a much poorer activity was exhibited by pure CeO_2 , with a NO conversion of less than 50% across the entire test range. In addition, the appearance of a negative NO conversion at 500°C reflects the occurrence of serious NH_3 oxidation [32], which is also compatible with the very poor N_2 selectivity (Figure 7b). Clearly, the introduction of sulfate species distinctly promotes the catalytic performance. S-CeS shows a more pronounced improvement in reaction efficiency than B-CeS, which acquires more than 90% NO conversion in the high-temperature range of $350\text{--}450^\circ\text{C}$. When the reaction temperature is further increased, a distinct deactivation was observed for both samples. However, the negative NO conversion was no longer present, demonstrating efficient suppression of NH_3 oxidation via sulfate modification. From the results of the activity test, we can tentatively propose that surface sulfates contribute more to promoting high-temperature SCR activity than bulk sulfates. To further confirm this, a direct comparison of the activity from B-CeS and B-CeS-W was achieved by taking advantage of the complete removal of bulk sulfates in the B-CeS-W sample. From Figure 7c, we can see that the catalytic performance at $400\text{--}500^\circ\text{C}$ shows negligible declining after removal of bulk sulfates, although obvious differences in low temperature range are displayed. This can be viewed as solid evidence that in com-

parison with surface sulfates, the contribution from bulk sulfates in boosting the catalytic performance of CeO_2 at high temperatures is insignificant.

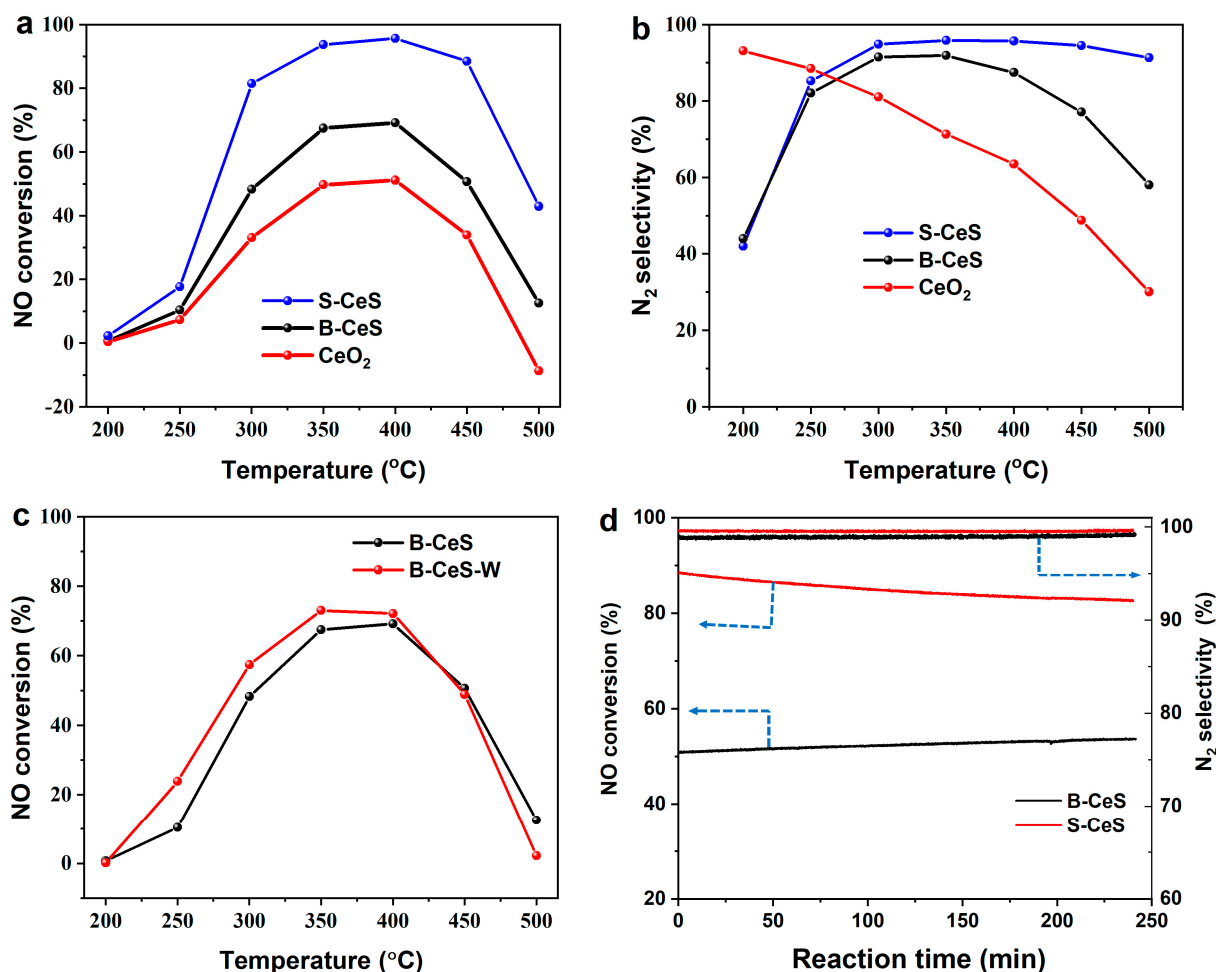


Figure 7. Effect of different sulfate species on the catalytic performance of CeO_2 in NH_3 -SCR. (a) NO conversion of S-CeS, B-CeS and CeO_2 , (b) N_2 conversion of S-CeS, B-CeS and CeO_2 , (c) NO conversion of B-CeS and B-CeS-W, (d) N_2 conversion of B-CeS and B-CeS-W.

To further explore the reaction stability of catalysts operated at high temperatures, the results of NO conversion/ N_2 selection as a function of reaction time are presented in Figure 7d. Both catalysts exhibit no obvious activity and selectivity change after successive operation at 450 °C for 240 min, revealing a good reaction stability of the sulfated samples.

2.6. The Acidity of Prepared Catalysts (NH_3 -TPD)

To disclose possible reasons for the different catalytic behaviors of surface and bulk sulfates in promoting high-temperature NH_3 -SCR performance, the acid and redox properties were explored. Figure 8 presents the NH_3 -TPD results. In line with previous studies, both catalysts showed a wide range of NH_3 desorption [22,24]. Through further examination, two desorption peaks can be differentiated. The low-temperature desorption with a peak centered at 150 °C can be attributed to NH_3 adsorbed on the weak acid sites from CeO_2 . It is well reported that due to the nature of basicity, pure CeO_2 possesses weak acidity. With introduction of sulfate species, the acidity is strongly enhanced, as evidenced by the appearance of another desorption peak at a temperature of 263 °C.

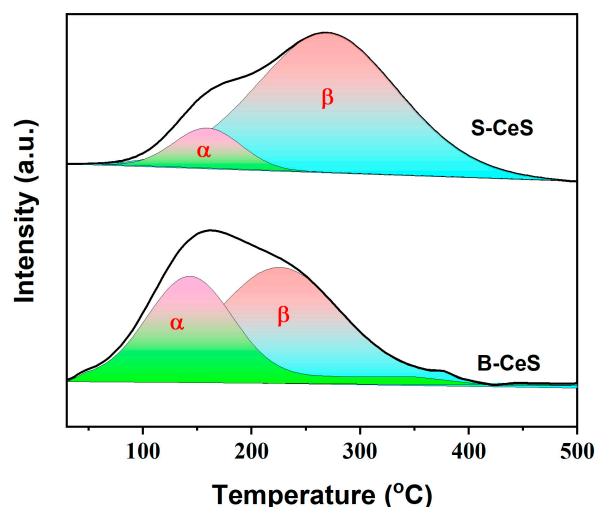


Figure 8. The NH_3 -TPD profiles of B-CeS and S-CeS.

Interestingly, despite their comparable sulfate content, the distribution of weak and strong acid sites over the two catalysts varies sharply. For B-CeS, weak acidity is dominant, as can be deduced from the appearance of a maximum NH_3 desorption signal at 150 °C (peak α). In view of the fact that insufficient contact is present between sulfate species and CeO_2 , more surface sites from ceria can be provided for NH_3 adsorption. On the other hand, due to the aggregation state of sulfate in B-CeS, fewer sites from sulfates are available for NH_3 adsorption. It is reasonable that this changes when bulk sulfates are substituted by surface sulfates. From the XPS and H_2 -TPR results, we know that abundant sulfates are bound to the CeO_2 surface. With this significant difference in sulfate species distribution, we can reasonably conclude that the amount of strong acid sites (peak β) increases at the expense of the weak sites provided by CeO_2 .

2.7. The Oxidation Properties with Respect to NO and NH_3 (NO Oxidation and NH_3 Oxidation)

The oxidation properties of catalysts with respect to reactants are investigated in terms of NO oxidation and NH_3 oxidation. The NO oxidation performance is shown in Figure 9a. In general, both catalysts show poor activity in converting NO to NO_2 , which is evidenced by the high temperature required to initiate the reaction (250 °C and the obtained poor maximum conversion efficiency (<20%). It has been previously reported that although ceria has excellent redox properties, it shows poor NO oxidation performance and, due to the strong electron-withdrawing effect from S=O in sulfate group, the modification of sulfate species can induce a further deterioration in NO oxidation performance [30]. From this point of view, it is reasonable that the B-CeS displayed a better NO oxidation performance than the S-CeS, since the main body of ceria is less disrupted by bulk sulfates in B-CeS. By comparing the NO oxidation performance with the high-temperature NH_3 -SCR results, we can conclude that the ability to oxidize NO is not responsible for the different SCR behaviors at high temperatures.

The results of the $\text{NH}_3 + \text{O}_2$ test are shown in Figure 9b. In line with the NO oxidation performance, the S-CeS catalyst presents a worse oxidation capacity for NH_3 . It is possible that due to the strong coverage of sulfate species on CeO_2 , the inherent surface oxygen on ceria is not available for S-CeS. As a result, a poor oxidation ability is exhibited, which can suppress ammonia oxidation to some extent at high temperatures. Based on the above analysis, we can conclude that in addition to the change in acid sites, the reduced oxidation capacity of reductant NH_3 constitutes another reason for the better performance of the S-CeS sample in high-temperature NH_3 -SCR.

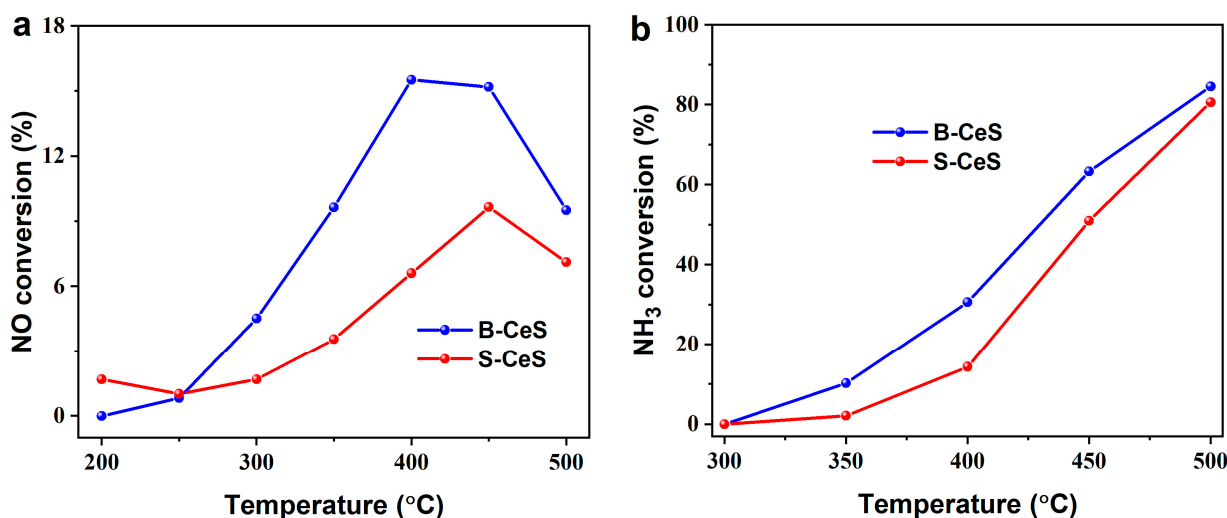


Figure 9. (a) NO oxidation and (b) NH₃ oxidation results of B-CeS and S-CeS.

3. Materials and Methods

3.1. Catalyst Preparation

CeO₂ modified with bulk sulfates was constructed through a novel top-down strategy. Ce₂(SO₄)₃·xH₂O was employed directly as the precursor, and with help of a harsh thermal treatment (static air, 900 °C, 1 h), most of the metal salt was converted into CeO₂. Notably, a minute amount of precursor was not decomposed and still existed as bulk phase in the mixture. For simplicity, the obtained sample is denoted as B-CeS.

The CeO₂ modified with surface sulfates was obtained via a vapor sulfation method. Pure CeO₂ derived from thermal treatment of cerium nitrate hydrate (900 °C, 1 h) was exposed to a stream of 2000 ppm SO₂ + O₂ to obtain the designated sample of CeO₂ modified with surface sulfate (S-CeS). By controlling the treatment time, a similar value in sulfate content as B-CeS is guaranteed.

A designed experiment of water leaching was performed to discriminate bulk sulfates and surface sulfates, by taking advantage of their different behaviors in water solubility. The B-CeS and S-CeS catalysts were dropped into distilled water, washed to remove the soluble sulfates, sonicated, filtered and dried to obtain the water-washed samples, which are named B-CeS-W and S-CeS-W, respectively.

3.2. Catalyst Characterization

The specific surface area was characterized using the N₂ sorption technique at −196 °C on an Micromeritics ASAP-2020 adsorption apparatus (Norcross, GA, USA). The samples were vacuum-pretreated at 300 °C for 3 h before measurement.

TG was performed on a Netzsch thermal analyzer STA 449C (Erich NETZSCH GmbH & Co.Holding KG, Selb, Germany) with N₂ as carrier gas and a test temperature range of 0–1000 °C with a temperature rise rate of 10 °C/min.

Surface morphologies of the catalyst samples were investigated using a FEI NANO SEM430 (Fei company, Lausanne, Switzerland) scanning electron microscope. All SEM images were obtained from secondary electrons with an accelerating voltage of 15 kV. The elemental composition and distribution were determined using an Oxford X-Max20 EDS equipment (Oxford Instruments Private Limited, Oxford, UK).

Raman spectra of samples were collected on a LabRAM Aramis (Japan Hobiba, Kyoto, Japan) Laser Raman spectroscopy with a 532 nm Ar⁺ laser beam.

XRD was performed on a Philips X'pert Pro diffractometer (Philips Analytical, Overijssel, The Netherlands) with a Ni filter and a Cu target K_α radiation source (wavelength 0.15418 nm). The operating voltage and current were set to 40 kV and 40 mA, and data were collected in the range 2θ = 10–80° with a scanning speed of 10 °C/min.

XPS was performed on a PHI 5000 VersaProbe X-ray photoelectron spectrometer (PHI Corporation, Kanagawa, Japan) with a monochromatic Al K_{α} radiation source (1486.6 eV) and an acceleration power of 15 kW. Prior to testing, the sample was degassed to below 5×10^{-7} Pa at room temperature in an ultra-high vacuum chamber. Sample charge effects were compensated for by correcting the C 1s spectrum to 284.6 eV. The accuracy of the binding energy was 0.1 eV.

Temperature-programmed reduction by H_2 (H_2 -TPR) was carried out in a quartz U-tube reactor connected to a thermal conduct detector (TCD) with an H_2 /Ar mixture (7% H_2 by volume) as a reductant. A total of 10 mg sample was used for each measurement. Before introducing it to the H_2 -Ar stream, the sample was pretreated in the N_2 stream at 200 °C for 1 h. The H_2 consumption profile was collected from room temperature to 900 °C at a rate of 10 °C/min.

The acid properties were determined from temperature-programmed desorption (TPD) of ammonia using a Nicolet IS10 FT-IR spectrometer (Thermo Scientific, Waltham, MA, USA) equipped with a 2 m path-length gas cell (2 L volume). Catalysts were evaluated in a fixed-bed quartz reactor (5 mm internal diameter) operating with a steady-state flow. About 100 mg sample was primarily pretreated using argon (100 mL/min) at 200 °C for 1 h, then it was cooled to room temperature and exposed to 500 ppm NH_3 /Ar (100 mL/min) for 1 h. Thereafter, excessive physical adsorbed ammonia was removed by purging with argon at room temperature for 1 h. All NH_3 -TPD tests were carried out by increasing the temperature from 30 to 600 °C at a rate of 10 °C/min and an argon flow rate of 100 mL/min.

The NH_3 /NO oxidation experiments were carried out on a fixed-bed reactor with a gas composition of 500 ppm NH_3 (or NO), 5 vol.% O_2 , and N_2 as equilibrium gas at a gas flow rate of 100 mL/min. A certain amount (200 mg) of the sample was loaded into the quartz tube reactor, purged with N_2 at 200 °C for 1 h and then cooled to room temperature. After the reaction gas was adsorbed to saturation, the reactions were carried out at different temperatures. The concentrations of NO and NH_3 were recorded online using a Thermofisher IS10 FTIR spectrometer, and the catalytic performance data as a function of temperature were collected after being kept stable for 30 min at each temperature point.

3.3. Activity Measurement

The catalytic performance was evaluated in a fixed-bed quartz reactor with 5 mm internal diameter under steady-state flow. The feed gas was 500 ppm NO, 500 ppm NH_3 , 5% O_2 , and total gas flow was controlled at 100 mL/min. The WHSV was 60,000 mL/(gh). A total of 100 mg catalyst was sieved through a 40–60 mesh. Before the tests, the catalyst was pretreated in a purified Ar stream at 200 °C for 30 min to avoid surface impurities. Then, the mixed gases were switched on and activity data were collected at every target temperature after stabilizing for 30 min in the range of 200–500 °C. The concentration of effluent gases was analyzed on a Nicolet IS10 FT-IR spectrometer equipped with a 2 m path-length gas cell (2 L volume). The NO conversion was calculated based on the following equations:

$$\text{NO conversion (\%)} = \frac{[NO]_{in} - [NO]_{out}}{[NO]_{in}} \times 100\%$$

$$N_2 \text{ selectivity (\%)} = \frac{[NO]_{in} - [NO]_{out} + [NH_3]_{in} - [NH_3]_{out} - [NO_2]_{out} - 2 \times [N_2O]_{out}}{[NO]_{in} - [NO]_{out} + [NH_3]_{in} - [NH_3]_{out}} \times 100\%$$

4. Conclusions

By explicitly controlling the existing states of sulfate species, the effect of surface and bulk sulfates on high-temperature catalytic performance of ceria in NH_3 -SCR was investigated in the present study. It was found that introduction of sulfate species induced

little modification on the bulk structure of CeO₂. However, both the adsorption and reaction behaviors were significantly altered. In comparison with pure CeO₂, introduction of sulfates notably enhanced the high-temperature NH₃-SCR performance. In addition, an apparent difference in reaction efficiency between surface and bulk sulfates was exhibited. Due to close contact between sulfate species and ceria, the active surface oxygen species from ceria were largely eliminated, resulting in alleviated NH₃ oxidation for S-CeS. On the other hand, the strong interaction between SO₂ and surface oxygen species from ceria created sufficient sulfate species. As a result, more strong acid sites were generated in S-CeS. With the obtainment of these unique properties (more strong acid sites and reduced NH₃ oxidation capacity), the catalyst of ceria modified with surface sulfates displayed enhanced catalytic performance in high-temperature NH₃-SCR.

Author Contributions: Conceptualization, C.T. (Changjin Tang) and C.T. (Chong Tan); methodology, C.T. (Chong Tan), Z.G., L.C. and J.J.; validation, C.T. (Chong Tan), Z.G., Y.W., B.Z. and L.C.; formal analysis, C.T. (Chong Tan), Z.G. and S.S.; investigation, C.T. (Chong Tan), L.C., H.Z., S.S., C.H. and L.L.; data curation, C.T. (Chong Tan), S.S., Y.W., H.Z. and B.Z.; writing—original draft preparation, C.T. (Chong Tan); writing—review and editing, C.T. (Chong Tan), C.T. (Changjin Tang) and S.S.; supervision, H.Z. and C.T. (Changjin Tang); project administration, C.T. (Changjin Tang); funding acquisition, C.T. (Changjin Tang). All authors have read and agreed to the published version of the manuscript.

Funding: This research was supported by the National Science Foundation of China (21976081, 21972062) and the Major Scientific and Technological Project of Bingtuan (2018AA002).

Data Availability Statement: Not applicable.

Acknowledgments: The financial support from the National Science Foundation of China (21976081, 22276097) is greatly acknowledged.

Conflicts of Interest: The authors declare no conflict of interest.

Glossary

S-CeS	CeO ₂ modified with surface sulfates
B-CeS	CeO ₂ modified with bulk sulfates
B-CeS-W	The B-CeS catalyst treated using water leaching
S-CeS-W	The S-CeS catalyst treated using water leaching

References

1. Han, L.; Cai, S.; Gao, M.; Hasegawa, J.-Y.; Wang, P.; Zhang, J.; Shi, L.; Zhang, D. Selective Catalytic Reduction of NO_x with NH₃ by Using Novel Catalysts: State of the Art and Future Prospects. *Chem. Rev.* **2019**, *119*, 10916–10976. [[CrossRef](#)]
2. Zhao, S.; Peng, J.; Ge, R.; Wu, S.; Zeng, K.; Huang, H.; Yang, K.; Sun, Z. Research progress on selective catalytic reduction (SCR) catalysts for NO removal from coal-fired flue gas. *Fuel Process. Technol.* **2022**, *236*, 107432. [[CrossRef](#)]
3. Kobayashi, M.; Miyoshi, K. WO₃-TiO₂ monolithic catalysts for high temperature SCR of NO by NH₃: Influence of preparation method on structural and physico-chemical properties, activity and durability. *Appl. Catal. B* **2007**, *72*, 253–261. [[CrossRef](#)]
4. Lian, Z.; Deng, H.; Xin, S.; Shan, W.; Wang, Q.; Xu, J.; He, H. Significant promotion effect of the rutile phase on V₂O₅/TiO₂ catalysts for NH₃-SCR. *Chem. Commun.* **2021**, *57*, 355–358. [[CrossRef](#)] [[PubMed](#)]
5. Feng, S.; Li, Z.; Shen, B.; Yuan, P.; Wang, B.; Liu, L.; Wang, Z.; Ma, J.; Kong, W. High activity of NH₃-SCR at high temperature over W-Zr/ZSM-5 in the exhaust gas of diesel engine. *Fuel* **2022**, *323*, 124337. [[CrossRef](#)]
6. Park, S.; Choi, G.M.; Tanahashi, M. Demonstration of a gas turbine combustion-tuning method and sensitivity analysis of the combustion-tuning parameters with regard to NO_x emissions. *Fuel* **2019**, *239*, 1134–1142. [[CrossRef](#)]
7. Cao, L.; Wu, X.; Xu, Y.; Lin, Q.; Hu, J.; Chen, Y.; Ran, R.; Weng, D. Ceria-modified WO₃-TiO₂-SiO₂ monolithic catalyst for high-temperature NH₃-SCR. *Catal. Commun.* **2019**, *120*, 55–58. [[CrossRef](#)]
8. Topsoe, N.Y. Mechanism of the selective catalytic reduction of nitric oxide by ammonia elucidated by in situ on-line fourier transform infrared spectroscopy. *Science* **1994**, *265*, 1217–1219. [[CrossRef](#)]
9. Topsoe, N.Y.; Dumesic, J.A.; Topsoe, H. Vanadia-Titania Catalysts for Selective Catalytic Reduction of Nitric-Oxide by Ammonia. *J. Catal.* **1995**, *151*, 241–252. [[CrossRef](#)]
10. Imanari, M.; Watanabe, Y. Reduction of NO_x in combustion flue gases on tungsten based catalysts. In *Studies in Surface Science and Catalysis*; Elsevier: Amsterdam, The Netherlands, 1981; Volume 7, pp. 841–852.

11. Byrne, J.; Chen, J.; Speronello, B. Selective catalytic reduction of NO_x using zeolitic catalysts for high temperature applications. *Catal. Today* **1992**, *13*, 33–42. [[CrossRef](#)]
12. Xie, L.; Liu, F.; Ren, L.; Shi, X.; Xiao, F.-S.; He, H. Excellent performance of one-pot synthesized Cu-SSZ-13 catalyst for the selective catalytic reduction of NO_x with NH₃. *Environ. Sci. Technol.* **2014**, *48*, 566–572. [[CrossRef](#)] [[PubMed](#)]
13. Moon Lee, S.; Su Kim, S.; Chang Hong, S. Systematic mechanism study of the high temperature SCR of NO by NH₃ over a W/TiO₂ catalyst. *Chem. Eng. Sci.* **2012**, *79*, 177–185. [[CrossRef](#)]
14. Shan, W.; Liu, F.; Yu, Y.; He, H. The use of ceria for the selective catalytic reduction of NO_x with NH₃. *Chin. J. Catal.* **2014**, *35*, 1251–1259. [[CrossRef](#)]
15. Wu, T.; Guo, R.-t.; Li, C.-f.; Pan, W.-g. Recent progress of CeO₂-based catalysts with special morphologies applied in air pollutants abatement: A review. *J. Environ. Chem. Eng.* **2022**, *11*, 109136.
16. Tang, C.; Zhang, H.; Dong, L. Ceria-based catalysts for low-temperature selective catalytic reduction of NO with NH₃. *Catal. Sci. Technol.* **2016**, *6*, 1248–1264. [[CrossRef](#)]
17. Yi, T.; Zhang, Y.; Li, J.; Yang, X. Promotional effect of H₃PO₄ on ceria catalyst for selective catalytic reduction of NO by NH₃. *Chin. J. Catal.* **2016**, *37*, 300–307. [[CrossRef](#)]
18. Ji, J.; Han, L.; Song, W.; Sun, J.; Zou, W.; Tang, C.; Dong, L. Promotion effect of bulk sulfates over CeO₂ for selective catalytic reduction of NO by NH₃ at high temperatures. *Chin. Chem. Lett.* **2023**, *34*, 107769. [[CrossRef](#)]
19. Zhang, L.; Zou, W.X.; Ma, K.L.; Cao, Y.; Xiong, Y.; Wu, S.G.; Tang, C.J.; Gao, F.; Dong, L. Sulfated Temperature Effects on the Catalytic Activity of CeO₂ in NH₃-Selective Catalytic Reduction Conditions. *J. Phys. Chem. C* **2015**, *119*, 1155–1163. [[CrossRef](#)]
20. Xie, R.; Ma, L.; Li, Z.; Qu, Z.; Yan, N.; Li, J. Review of sulfur promotion effects on metal oxide catalysts for NO_x emission control. *ACS Catal.* **2021**, *11*, 13119–13139. [[CrossRef](#)]
21. Lian, Z.; Shan, W.; Wang, M.; He, H.; Feng, Q. The balance of acidity and redox capability over modified CeO₂ catalyst for the selective catalytic reduction of NO with NH₃. *J. Environ. Sci.* **2019**, *79*, 273–279. [[CrossRef](#)]
22. Chen, J.; Zhao, W.; Wu, Q.; Mi, J.; Wang, X.; Ma, L.; Jiang, L.; Au, C.; Li, J. Effects of anaerobic SO₂ treatment on nano-CeO₂ of different morphologies for selective catalytic reduction of NO_x with NH₃. *Chem. Eng. J.* **2020**, *382*, 122910. [[CrossRef](#)]
23. Tan, W.; Wang, J.; Yu, S.; Liu, A.; Li, L.; Guo, K.; Luo, Y.; Xie, S.; Gao, F.; Liu, F.; et al. Morphology-Sensitive Sulfation Effect on Ceria Catalysts for NH₃-SCR. *Top. Catal.* **2020**, *63*, 932–943. [[CrossRef](#)]
24. Ji, J.; Jing, M.; Wang, X.; Tan, W.; Guo, K.; Li, L.; Wang, X.; Song, W.; Cheng, L.; Sun, J.; et al. Activating low-temperature NH₃-SCR catalyst by breaking the strong interface between acid and redox sites: A case of model Ce₂(SO₄)₃-CeO₂ study. *J. Catal.* **2021**, *399*, 212–223. [[CrossRef](#)]
25. Yao, X.; Wang, Z.; Yu, S.; Yang, F.; Dong, L. Acid pretreatment effect on the physicochemical property and catalytic performance of CeO₂ for NH₃-SCR. *Appl. Catal. A* **2017**, *542*, 282–288. [[CrossRef](#)]
26. Chen, S.; Xie, R.; Liu, Z.; Ma, L.; Yan, N. Efficient NO_x Reduction against Alkali Poisoning over a Self-Protection Armor by Fabricating Surface Ce₂(SO₄)₃ Species: Comparison to Commercial Vanadia Catalysts. *Environ. Sci. Technol.* **2023**, *57*, 2949–2957. [[CrossRef](#)] [[PubMed](#)]
27. Xie, Q.; Cai, Y.; Zhang, L.; Hu, Z.; Li, T.; Wang, X.; Zeng, Q.; Wang, X.; Sun, J.; Dong, L. Relationships between Adsorption Amount of Surface Sulfate and NH₃-SCR Performance over CeO₂. *J. Phys. Chem. C* **2021**, *125*, 21964–21974. [[CrossRef](#)]
28. Jin, R.; Liu, Y.; Wu, Z.; Wang, H.; Gu, T. Relationship between SO₂ poisoning effects and reaction temperature for selective catalytic reduction of NO over Mn-Ce/TiO₂ catalyst. *Catal. Today* **2010**, *153*, 84–89. [[CrossRef](#)]
29. Shu, Y.; Aikebaier, T.; Quan, X.; Chen, S.; Yu, H. Selective catalytic reaction of NO_x with NH₃ over Ce-Fe/TiO₂-loaded wire-mesh honeycomb: Resistance to SO₂ poisoning. *Appl. Catal. B* **2014**, *150*, 630–635. [[CrossRef](#)]
30. Ji, J.; Gao, N.; Song, W.; Tang, Y.; Cai, Y.; Han, L.; Cheng, L.; Sun, J.; Ma, S.; Chu, Y. Understanding the temperature-dependent H₂O promotion effect on SO₂ resistance of MnO_x-CeO₂ catalyst for SCR denitration. *Appl. Catal. B* **2023**, *324*, 122263. [[CrossRef](#)]
31. Waqif, M.; Bazin, P.; Saur, O.; Lavalle, J.C.; Blanchard, G.; Touret, O. Study of ceria sulfation. *Appl. Catal. B* **1997**, *11*, 193–205. [[CrossRef](#)]
32. Gu, T.; Liu, Y.; Weng, X.; Wang, H.; Wu, Z. The enhanced performance of ceria with surface sulfation for selective catalytic reduction of NO by NH₃. *Catal. Commun.* **2010**, *12*, 310–313. [[CrossRef](#)]
33. Giordano, F.; Trovarelli, A.; de Leitenburg, C.; Giona, M. A Model for the Temperature-Programmed Reduction of Low and High Surface Area Ceria. *J. Catal.* **2000**, *193*, 273–282. [[CrossRef](#)]

Disclaimer/Publisher's Note: The statements, opinions and data contained in all publications are solely those of the individual author(s) and contributor(s) and not of MDPI and/or the editor(s). MDPI and/or the editor(s) disclaim responsibility for any injury to people or property resulting from any ideas, methods, instructions or products referred to in the content.